ICANS XIX,
19th meeting on Collaboration of Advanced Neutron Sources
March 8 – 12, 2010
Grindelwald, Switzerland

Imaging experiments on NOBORU at MLF

M. Harada, K. Oikawa, M. Ooi, T.Kai, K.Sakai, F. Maekawa and N. Watanabe
T. Shinohara and S. Takata
J-PARC Center, JAEA, Tokai-mura, Naka-Gun, Ibaraki-ken, 319-1195, Japan

ABSTRACT

Recent years, an energy-selective neutron imaging method as radiography has been developed using pulsed neutron sources in the world. In this method, much additional information can be obtained by using resonance absorption transmission, Bragg edge transmission, and so on. Preliminary experiments on the energy-selective neutron imaging have been performed using an instrument NOBORU at JSNS/MLF in J-PARC. First of all, the neutron field (spectral intensity and spatial distribution) at the sample position of NOBORU was measured. Then a preliminary test of the resonance absorption transmission with typical samples was performed to know the sensibility of the measurement. As an example of Bragg edge transmission imaging, samples of friction welding rods of stainless steel-invar alloy and aluminum alloy-invar alloy were measured. As a final example, a test experiment using polarized neutrons was done to measure the magnetic field. From these experiments the energy-selective neutron imaging was confirmed to be useful and the NOBORU beam line was concluded to be suitable for the energy-selective imaging as the experimental site.

1. Introduction

1.1. Energy-selective imaging in J-PARC

Neutron radiography at reactor sources is one of the established techniques for seeing the inside of an object material nondestructively. Recent years, so-call "Energy-selective imaging" has been developed in the world,. For example, several papers about the energy-selective imaging were reported from PSI (Paul-Scherrer Institute, Swiss) and TUM (Technische Universität München, Germany). Here, we call imaging as radiography with something additional, for example, resonance absorption, Bragg edge, and so on. There is so far no dedicated beam line in pulsed spallation neutron source in the world for this purpose. However, the designs toward the construction of the dedicated beam line start in ISIS in RAL (Rutherford Appleton Laboratory, UK), SNS in ORNL (Oak Ridge National Laboratory, USA) and J-PARC (Japan Proton Accelerator Research Complex, Japan). We are developing this technique in collaboration with Hokkaido University, Quantum Beam Science Directorate and Nuclear Science and Engineer Directorate in JAEA.

In Japan, a MW-class pulsed spallation neutron source (JSNS) has been constructed and is in operation since May 2008. JSNS has a mercury (Hg) target and three super-critical 100%-para hydrogen moderators [1-3]. A proton beam with 3GeV and 25 Hz hits the Hg target. At the present stage, the proton beam power has reached at 120kW and is gradually increasing toward the final goal of 1MW. In JSNS, 23 neutron beam ports are equipped and 12 neutron beam line instruments are available as of March, 2010. NOBORU (NeutrOn Beam-line for Observation and Research Use) [4, 5] is one of the instruments in JSNS and is located at the beam line 10 (BL10) viewing the decoupled moderator. We built NOBORU to measure the neutronic performance of JSNS. NOBORU is also useful for developing a new measuring method, new components and new instruments. The energy-selective imaging is one of examples. Therefore, we confirmed

the suitability of NOBORU for the energy-selective imaging, and performed test experiments on the imaging using NOBORU. This paper describes preliminary results.

1.2. Brief description of NOBORU and merit for neutron imaging experiments

The concept and the expected performance of NOBORU have been reported in Ref. [1] and [2] in detail. Figure 1 shows a schematic view of NOBORU with a related part of JSNS. The sample position in the experimental space from the moderator is 14 m. Since it is shorter than those of the other instruments, a large epithermal neutron intensity and a wide energy range are available. Neutron beam is transported in a vacuum duct with a cross-section of 10 x 10 cm^2, which is the largest of all the instruments in JSNS. The large duct size brings high neutron intensity and large irradiation field. NOBORU furnishes a couple of sintered B_4C beam slits (0.5 cm in thickness) at 7.0 m and 12.7 m, a removable collimator made of steel and polyethylene at 12.5 m. A remote controlled rotary collimator (RC) is installed at 7.5 m position. The RC consists of steel (34.7 cm in length) and polyethylene (5 cm in length), and it has 4 different collimator sizes; Free (RC(F), 10 x 10 cm^2), Large (RC(L), 3.16 x 3.16 cm^2), Middle (RC(M), 1.78 x 1.78 cm^2) and Small (RC(S), 1.00 x 1.00 cm^2). These slits and collimators are useful for the control of L/D ratio and intensity. A T_0 chopper is planned to be installed at around 10 m position to eliminate the flush neutrons and gamma-ray. NOBORU has enough shielding to treat 10 x 10 x 10 cm^3 iron sample [6] and an adequate experimental space. It is suitable to treat a large size sample.

2. Experimental Methods

The measurement of intensity and spatial distribution of neutron field at the sample position of NOBORU is important for planning the imaging experiments. If there are any poor intensity areas in the spatial distribution, poor statistical precision would partially be occurred in a measurement. For measurements of the neutron spectral intensities, two zero-dimensional He-3 conventional counters were used. One of the He-3 counters was 10 x 10 cm^2 in lateral sizes with the efficiency of 10^{-5} at 25.3 meV and another was 1.27 cm in diameter and was filled with He-3 gas at 7 atm.

A neutron sensitive Imaging Plate (IP) was used for a measurement of spatial distribution of thermal neutrons with the high resolution. To measure a neutron-energy dependent spatial distribution, a position sensitive photomultiplier-tube with ZnS scintillator (RPMT) was used. A diameter of RPMT was 12.7 cm.

RPMT was used also for test experiments on the energy-selective imaging,

3. Results and discussions

3.1. Spectral intensity and effect of rotary collimator and Bi filter

Figure 2 shows measured neutron spectral intensity at the sample position. It was confirmed that the neutron intensity in the energy region below 100 meV was about 2.9 x 10^7 n/cm^2 at 1MW. This value corresponds to about 1/5 of the intensity at a beam line for the radiography in the JRR-3 reactor source. It was also confirmed that for a resonance absorption transmission measurement the intensity in the epithermal region was higher than that of the reactor source and neutrons at much higher energy than that in the reactor source can be observed.

To study a signal to noise ratio (S/N ratio) an ASTM standard sample [7], as shown in left figure in Fig. 3, was measured with collimators of various sizes. L/D means the collimation ratio related to the beam divergence and a larger L/D causes a smaller

divergence beam. Values of L/D in the case of RC(F), RC(L), RC(M) and RC(S) are 140, 190, 340 and 600, respectively. Right figure in Fig. 3 shows the result of the transmission of the ASTM sample measured by IP for the change of the RC size. For a comparison, similar measurement with the same size B_4C slit was performed as shown in the figure. In the case of the RC, transmission peaks from the ASTM sample are clear even for a smaller RC size due to higher L/D. Especially, even in the RC(S) (L/D=600) case, the transmission peaks are clearly observed (good S/N ratio). On the other hand, the B_4C slit case is not clear due to the transparent B_4C slit against the higher energy neutrons and gamma-rays. Note that, in the smaller B_4C slit case, neutrons as the signal become smaller and IP is sensitive to gamma rays, resulting in a very high background (not good S/N ratio).

Figure 4 shows the relation of the spectral intensity against the RC and the B_4C slit size. High energy ends, in which the measured intensities go down quickly due to the dead time loss caused by fast neutron and gamma ray flush, increase toward higher energy for larger slit cases, especially in the RC case. In the B_4C slit case, since the slit becomes more transparent with higher energy, increasing the high energy ends as observed in the RC case is hardly observed. The result indicates that the RC decreases the fast neutron and gamma-ray flush for larger slit cases. The measured intensities of thermal and epi-thermal neutrons also decrease with the relation to the slit size in the RC and the B_4C slit cases. Those are approximately in agreement with the calculated one for both cases, though it is not depicted.

To reduce the fast neutron and the gamma ray flush, the effect of a single crystal Bismuth (Bi) filter was studied. Especially, it is expected that the Bi filter is effective to decrease gamma rays due to a high atomic number material. The Bi filter of 2.54 cm in thickness is located at 12.6 m. Figure 5 shows the results, showing that the intensity at a higher energy region decreases being thermal neutron region almost unchanged. The results indicate that Bi filter is useful for the imaging on the viewpoint of avoiding or decreasing the fast neutron and gamma-ray flush.

3.2. Spatial distribution

Spatial distribution at the sample position is important for the planning of the measurement. Generally, as the energy selective imaging, the two-dimensional transmission data with a sample is divided by that without a sample in order to make influence of a neutron spatial distribution small. However, if there are any poor neutron intensity regions in the spatial distribution, statistical errors in those regions increase. Figure 6 shows the result of the neutron spatial distribution integrated in the energy region from 1 meV to 10 meV. In the measurement, RPMT was used. The B_4C slit located at 12.7 m was used with a square hole of 0.5 x 0.5 cm^2, like a pin hole. The result indicates that the spatial distribution has almost flat and symmetrical around the beam center. From the IP measurement result, when the hole size becomes larger, the spatial distribution becomes flatter.

Figure 7 shows the result of the neutron spatial distribution integrated in the epithermal region, 10 eV - 100 eV, showing non-uniform distribution reflecting non-uniform source neutron distribution in the moderator. When the resonance absorption transmission is used, such a distribution should be considered to avoid poor intensity (poor statistical precision).

3.3. Resonance absorption transmission

As test experiments of the resonance absorption transmission, some materials were measured using a Li-glass scintillation counter. Left figure in Fig. 8 shows a result on the soda glass transmission spectrum. Resonance dip of Na at 2.8 keV is clearly observed, although a quantitative analysis has not yet done. If a time resolution in the measurement is improved to be much below 1 μs, we guess that a detectable energy increases to be beyond 10 keV. Right figure in Fig. 8 shows a transmission spectrum of Ta foils, showing that in case of material including a strong resonance element a small sample of 10 μm can be clearly measured. We guess that in the Ta foil case the sample of a few μm in thickness is detectable. As another example, two stainless steel samples, SS304 and SS316, were measured. The result is shown in left figure in Fig. 9. Extra dips at 44.9 eV of Mo-95 contained in the 316 stainless steel can be observed, though it can not be observed in the 304 stainless steel. The result indicates that alloys can be distinguished with different dip by the consisted materials, even if they are very small composition. Examples are Nb and Mn in the stainless steels, and are Ti, Bi and Zr in the aluminum alloy. Right figure in Fig. 9 shows measured and calculated resonance absorption spectra for a Ta foil of 100 μm in thickness. There is a small discrepancy between both spectra, especially at the bump around 10eV. Though to consider the origin of the bump the elastic part of the resonance dip was calculated, the reason of the bump is not still understood. Therefore, further studies should be done in detail.

3.4. Bragg edge transmission

As an example of Bragg edge transmission, two friction welding rod samples of a stainless steel-invar alloy and aluminum alloy-invar alloy were measured. These samples for tensile strength tests have a cross section of 0.4 x 0.4 cm^2. Figure 10 shows two dimensional views of the Bragg edge transmission around 4.5 Å for both welded samples. Different regions can be distinguished by the transmission in the aluminum alloy-invar alloy case. TOF spectra for both samples in pure material region and close to the welding region are shown in Fig. 11, showing that pure regions and regions close to welding in both materials are distinguishable. Dips around 4.2 Å are typical Bragg edges. Above 4.2 Å, absorption reactions are mainly observed due to beyond maximum of the Bragg edge wave length. In the aluminum alloy case, the Bragg edge is not clear due to small cross section. In the regions close to the welding in the all cases, the Bragg edge patterns become small. The reason is that the crystallization of the alloy is changed by welding.

3.5. Polarized neutron transmission

As an example of the polarized neutron transmission, we performed the experiment with a solenoid using the set-up shown in Fig. 12 left. In this experiment, polarized neutrons made by a polarizer go through a solenoid and into RPMT. When the solenoid has no magnetic field, all neutrons go through the solenoid to RPMT. However, if the solenoid has some magnetic fields, the incident neutrons to RPMT decrease due to the depolarization at the solenoid. The result is shown in middle and right figure for the cases without and with magnetic field, respectively. The result indicates that a magnetic field can be observed by a polarized neutron transmission.

4. Summary

We measured the neutron spectral intensities and the spatial distribution at the sample position of NOBORU. The rotary collimator and the Bi filter decrease gamma rays

and high energy neutrons, resulting in improving neutron field for imaging experiments using thermal and cold neutrons. From the results, we confirmed that NOBORU was also useful for the energy selective imaging experiment.

As examples, preliminary tests of resonance absorption transmission, Bragg edge transmission and polarized neutron transmission were performed. Good results toward future experiments were obtained.

In these measurements, we found that RPMT was difficult to measure in the high neutron intensity field. In near future, we will prepare Micro PIxel Chamber (μPIC) for neutron experiments. μPIC is one of micro pattern gas chamber with a micro-pixel electrode structure developed by Cosmic Ray Group in Kyoto University [8].

Acknowledgements

The rotary collimator was prepared by the support of "Quantum Beam Fundamation Development Program" provided by MEXT.

References

[1] Y. Ikeda, *J. Nucl. Mater.*, **343** (2005) 7.
[2] Y. Ikeda, *Nucl. Instr. Meth.*, **A 600** (2009) 1.
[3] M. Arai and F. Maekawa, *Nucl. Phys. News*, **19** (2009) 34.
[4] K. Oikawa, et al., *Nucl. Instr. Meth.*, **A 589** (2008) 310.
[5] F. Maekawa, et al., *Nucl. Instr. Meth.*, **A 600** (2009) 335.
[6] M. Harada, et al., to be published in *J. Nucl. Sci. Technol.*, (2010).
[7] ASTM E545-1, Standard Method for Determining Image Quality in Direct Thermal Neutron Radiographic Examination
[8] K. Miuchi, et al., *Nucl. Instr. Meth.*, **A 535** (2004) 535.

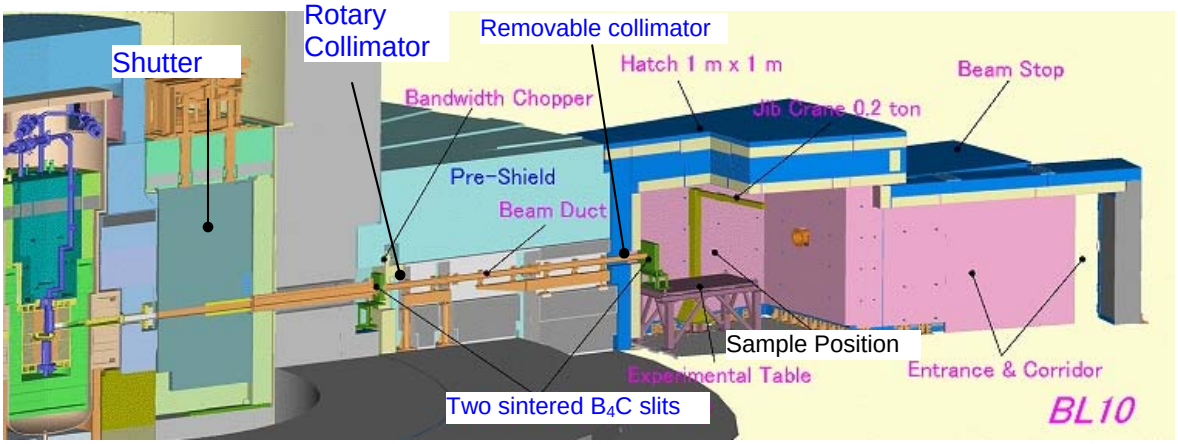

Fig.1 Schematic cross sectional view of NOBORU

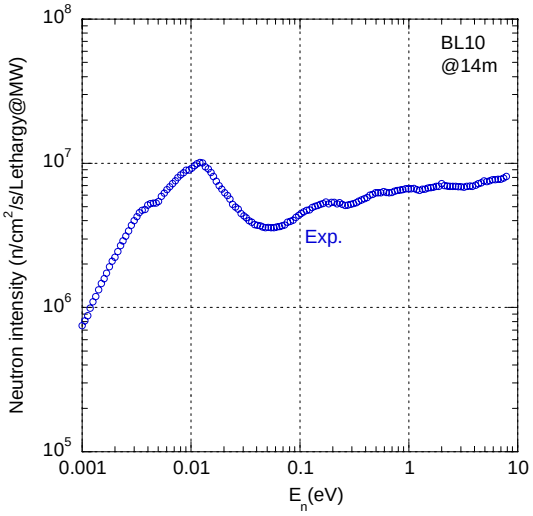

Fig.2 Measured neutron spectral intensity at sample position in NOBORU with the full open collimator. This value is converted to 1MW beam power.

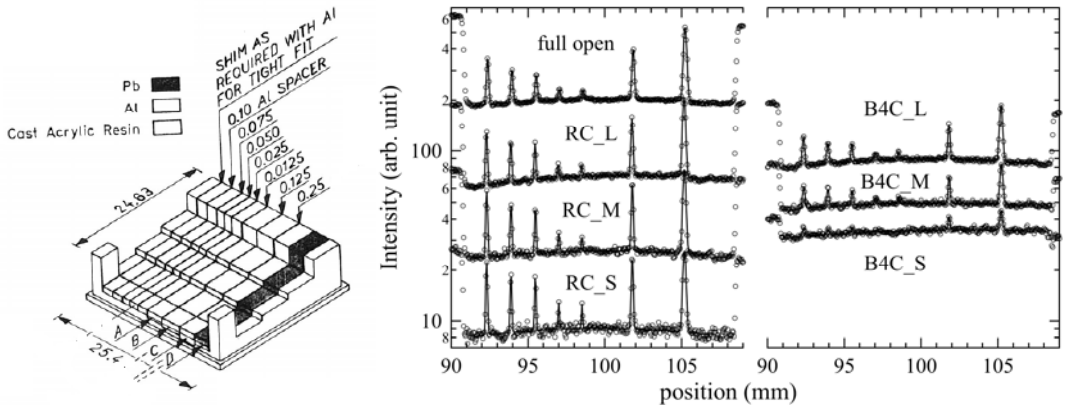

Fig. 3 The ASTM Standard sample (left) and beam pattern of it measured by IP (right)

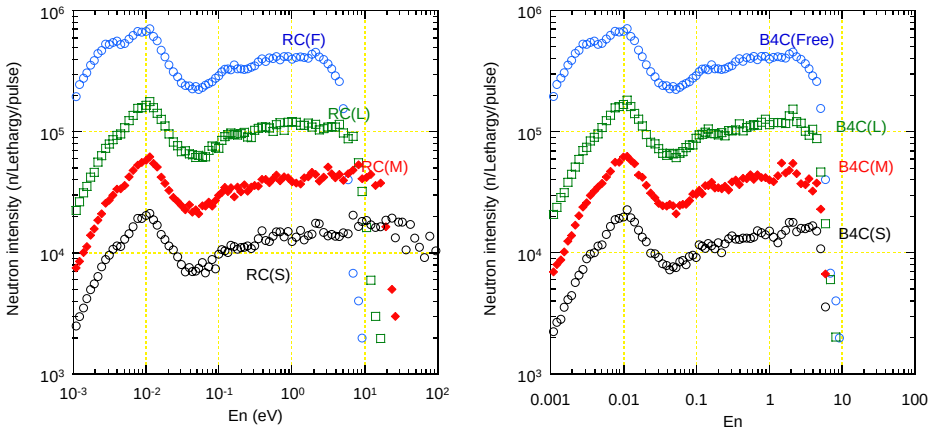

Fig. 4 Measured neutron spectral intensities in cases of various collimator sizes
Right and left figures are the cases of RC and B_4C slit, respectively.

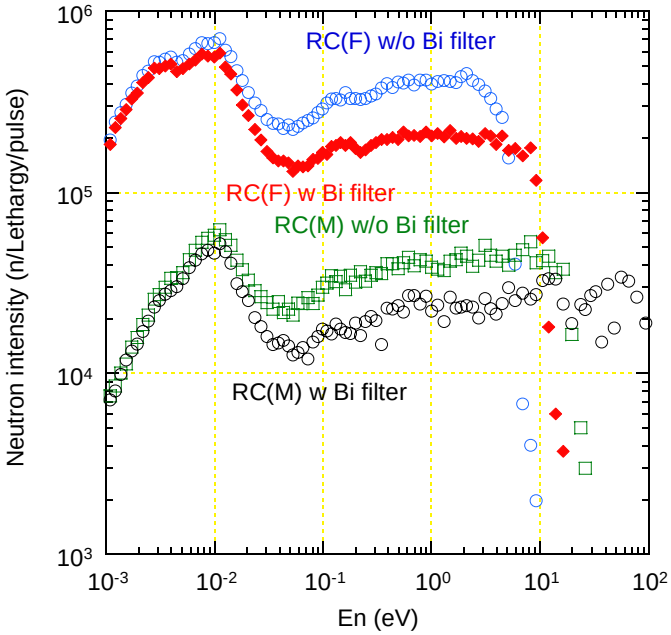

Fig. 5 Measured neutron spectral intensities in cases with and without Bi filter

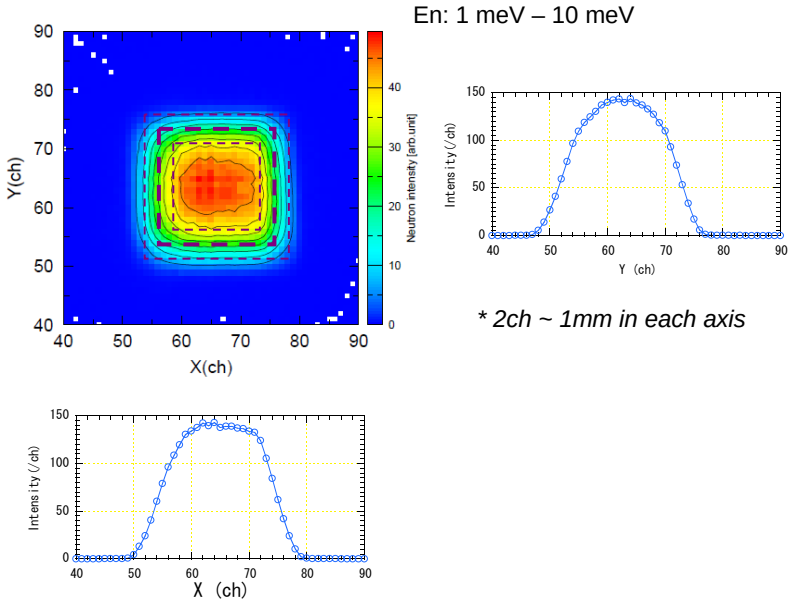

Fig.6 Spatial distribution in the energy region from 1 meV to 10 meV
Right and bottom figures are projection to horizontal and vertical center lines, respectively.

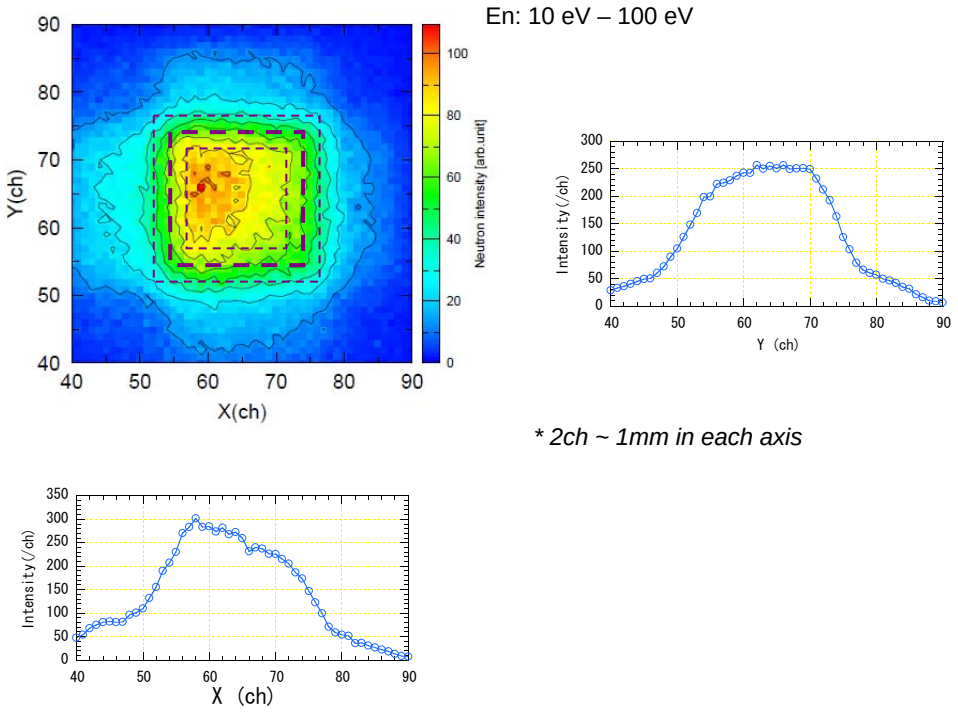

Fig.7 Spatial distribution in the energy region from 10 eV to 100 eV
Right and bottom figures are projection to horizontal and vertical center lines, respectively.

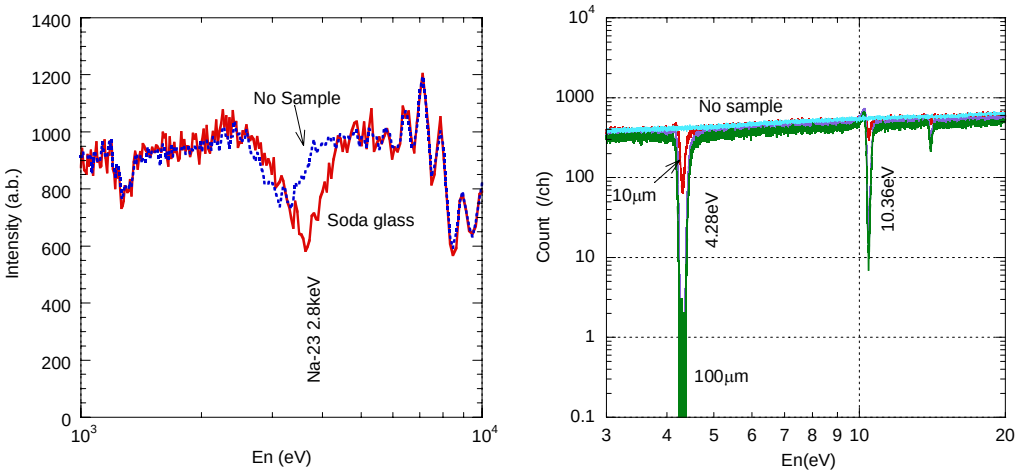

Fig. 8 Resonance absorption experiment (soda glass (left) and Ta foils (right))

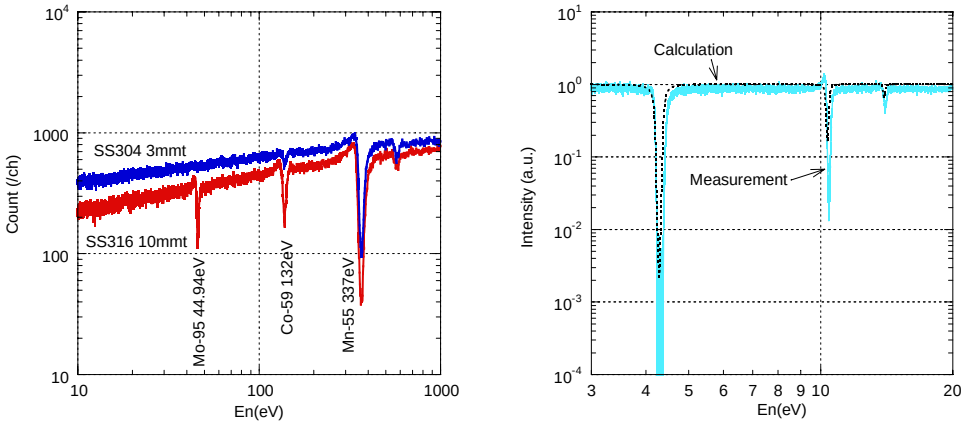

Fig. 9 Resonance absorption experiment
Left figure is transmission of stainless steel 304 and 316 samples.
Right figure is comparison of measured and calculated transmissions in Ta foil case.

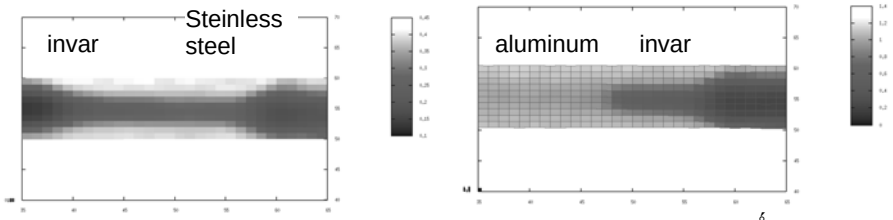

Fig. 10 Two-dimensional view of transmission around 4.5 Å
Left figure is stainless steel-invar sample and right figure is aluminum-Invar sample.

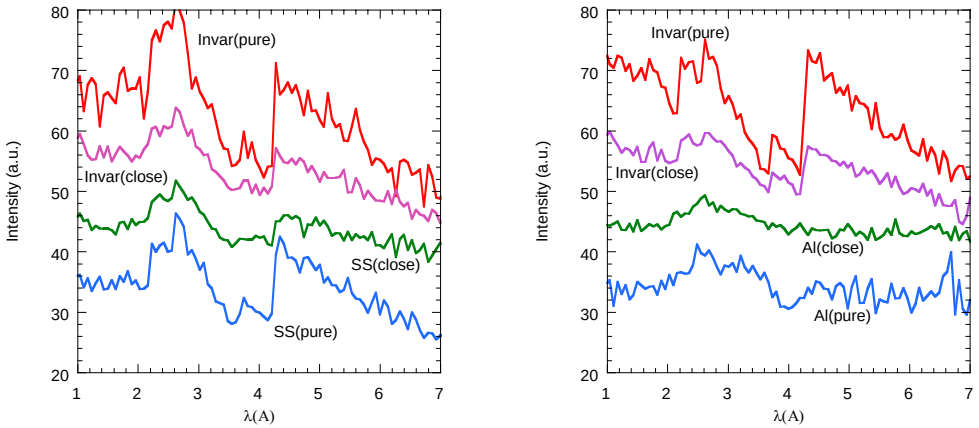

Fig. 11 Bragg edge transmission spectra
Left figure is stainless steel-invar sample and right figure is aluminum-Invar sample. The different spectra correspond to the different region of the sample (pure: pure material region, close: close to the welding region)

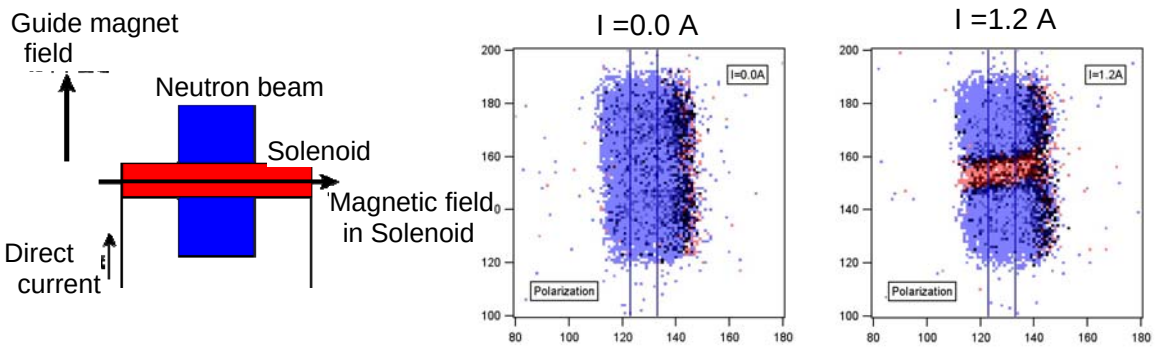

Fig. 12 Setup of polarized neutron transmission (Left) and
polarized neutron transmissions with (Right) and without (Middle) magnet filed